www.lajss.org
Latin American Journal of Solids and Structures 6 (2009) 131–152

Second-order plastic-zone analysis of steel frames Part I: Numerical formulation and examples of validation

Arthur R. Alvarenga and Ricardo A. M. Silveira*

Department of Civil Engineering, School of Mines
Federal University of Ouro Preto (UFOP) Campus Universitário
Morro do Cruzeiro, 35400-000 Ouro Preto, MG – Brazil

Abstract

This paper presents a second-order plastic-zone formulation for the non-linear analysis and design of plane steel frames with geometric imperfections and residual stress. The proposed numerical methodology has an inelastic formulation based on the plastic-zone method performed by the so-called "slice technique". This methodology also uses a beam-column finite element model based on the Bernoulli-Euler theory and described in the updated Lagrangian co-rotational system. The considered hypothesis and the adopted kinematic relation lead to an element stiffness matrix whose terms represent the constitutive law and second-order effects. An incremental-iterative Newton-Raphson strategy solves the global non-linear equation system and, at the internal force recovery level, in each iteration, an axial-force iterative process is proposed to obtain the axial-force balance at the element ends, more precisely determining the plasticity spread. Three benchmark structural problems are studied and the present work's findings validate the proposed numerical formulation and the axial-force iterative process. A companion paper discusses in depth the influence of geometrical imperfections and residual stress in steel frame design.

Keywords: Steel frames, Plastic-zone method, Non-linear analysis, Inelastic analysis, Element axial force

1 Introduction

Today every work on second-order inelastic analysis seems to claim that the development of computers caused the new steel-structure-design era to begin about twenty or, possibly, thirty years ago. However, remember that the usual design process, and probably the most popular of all time, is still the elastic first order analysis, conjugated with an isolated member's check using interactive formulas. For designing the beam-column member, it is necessary to define the effective length factor (K-factor used for member length correction) to simulate the condition of buckling, define the allowable stress during compression, and establish a link between the isolated member and structural system.

*Corresp. author email: ricardo@em.ufop.br Received 19 Mar 2009; In revised form 5 May 2009

The effective length *K-factor paradox* presented by Siat-Moy [28] contributed to a wave of researches showing several conditions under which traditional K-factors could not be precisely defined, failed to give a reasonable answer (over-estimates) or even worse, produced unsafe design.

New solutions or approximations intended to solve the aforementioned drawbacks, as well as others that appear to improve or modify the design process [5, 10, 18]. Giving the AISC point of view prevalent at the time, are works from LeMesurier [22], Hajjar [16], and Hajjar and White [17].

With the application of second-order elastic analysis, it is possible to detect the whole picture of slender structural system. Even in some structural cases, there is no need for the K factor at all (K = 1 [16]). Furthermore, this process is not computer-costly and there is a lot of available software that can perform this kind of analysis. Nevertheless, the main challenge is still to make some sort of second-order analysis by which the K-factor and member check are not obligatory.

Research along the last twenty years has brought new ways for the engineer to design without using the old methodology. Computer development paved the way for much research on non-linear methods with both elastic and inelastic approximations. As processor speed, graphic interfaces, software facilities, and memory capacity has expanded, the mathematical formulations and computing programs have grown more complex.

However, only after the publication of Australian Standard AS4100 [1] were designers explicitly allowed to check in-plane member and frame stability solely on a second-order inelastic analysis basis, named here *advanced analysis*. More recently, AISC [25] provided the option for evaluating overall frame stability without effective length factors. To use it, of course, one must know precisely what requirements to obey, so the first step is to define this kind of analysis.

Advanced analysis is a set of accurate second-order inelastic analyses that account for large displacements, plasticity spread and initial imperfection effects. The structural problem is analyzed in such a way that the strength or stability limit of the whole (or part of) system is determined precisely, so individual in-plane member checks are not required. It is a direct design.

There are two known research lines to develop a computational advanced *direct* analysis in steel framed structures, i.e.:

i. the refined plastic-hinge method, where scalar parameters and tangent modulus account for member rigidity degeneration, which diminishes section properties as soon as yield begins. This method provides good answers and does not require too much computer work [9, 23, 32]. In this context, Chan and Chui [6, 7] proposed a refined plastic-hinge method based on the section assemblage concept [20, 24];

ii. the plastic-zone method (PZ), where the structure is modeled using a refined mesh (members and sections) in such a way that plastic-zone formation can be monitored along the member's length, as well as its cross section. This method is very accurate but requires great computer effort. Clarke [11], Vinnakota and Foley [30], and Foley [13] followed

this approach. The Lavall [21] and Pimenta [27] works applied one approximation of this method called slice technique, which the present work also adopts [2, 3].

Besides being considered a complete second-order inelastic analysis, the computational advanced analysis must still fulfill the following minimum requirements:

i. rigorous mathematics formulation based on well-understood engineering theories of solid mechanics;

ii. structural model shall include the stability effects P-Δ and P-δ;

iii. member forces cannot violate the cross section strength: full plasticity condition;

iv. structural model must capture plasticity spread;

v. strength, deformations, and internal force distribution must be close to benchmark solutions;

vi. initial geometric imperfections and residual stress effects must be included in the analysis.

This paper presents a second-order plastic-zone formulation for the non-linear inelastic analysis and design of plane steel frames according to these requirements. Thus, the next section displays the numerical formulation, including the strain field, the finite element model, and the second-order inelastic stiffness matrix. The considered hypothesis and kinematic relations adopted lead to a beam-column element stiffness matrix whose terms represent the constitutive law and second-order effects. The standard incremental-iterative Newton-Raphson strategy solves the global non-linear equation system. This work also presents a new proposal: axial force iterative integration. This iterative process, developed at element level, aims to catch axial force balance when yield starts, which can more closely follow the plasticity spread. To validate this proposed numerical formulation, three steel structures are analyzed and some final remarks are presented in the last section.

A companion paper sheds some light on the last requirement stated above (material and geometric imperfections), called here *main aspects*. The initial geometric configurations, treated as a sum of the structure's out-of-plumbness and some member's out-of-straightness, coupled (or not), with residual stress effects, are studied on simple and very sensitive structures like portal frames.

2 The inelastic formulation

The plastic zone method defines every prismatic member as a finite element (FE) chain, as shown in Fig.1(a). All members (and its FEs) have uniform "I" cross sections. Figure 1(b) shows the mesh of these cross sections. Thus each FE, divided into a set of straight longitudinal rectangular strips called *slice*, provides the plasticity spread monitoring [26].

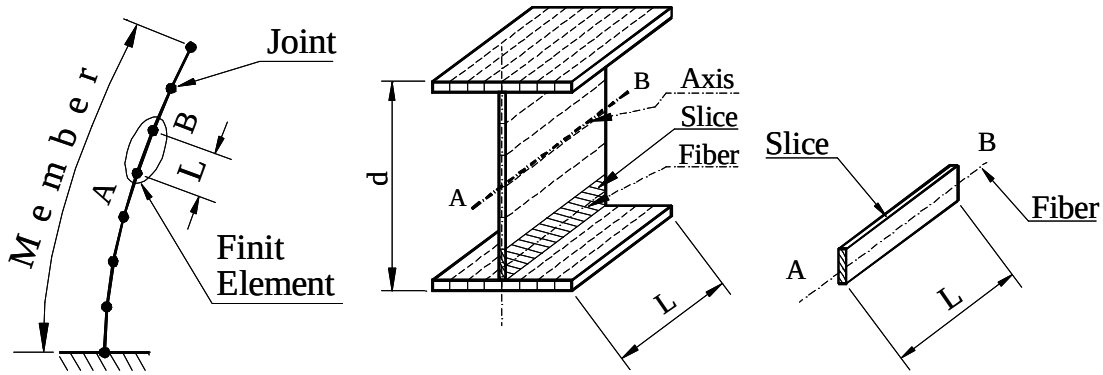

(a) Member: a set of FE. (b) FE in detail: a set of slices. (c) Slice monitored by fiber.

Figure 1: Plastic zone model.

The slice's centerline is named *fiber*, as shown in Fig.1(c). The slice technique assumes that, by evaluation of the fiber's stress-strain relation, it is possible to capture the state of each slice. So integrating the properties of the fiber from all slices along the section will update the section state, with the properties encountered on the two joints. This is similar to the moment-thrust-curvature integration procedure [15]. Hence, this establishes the FE state, giving the plastic-zone formation.

2.1 Strain field and finite element model

Considering that one fiber in the current state has L_c length, and turns to be L_d length in the deformed (or updated) state, as Fig.2(a) sketches, then the fiber stretching λ and its linear elongation can be defined by:

$$\lambda = \frac{L_d}{L_c} \tag{1a}$$

$$\varepsilon = \lambda - 1 \tag{1b}$$

Assuming a fiber to represent the slice as a whole, with slice's area A_s, where updated axial force N_d does fiber stretching, and also knowing the nominal (or Biot) stress σ and linear elongation ε energetically conjugate, the following relations can be written:

$$\sigma = \frac{N_d}{A_s} \tag{2a}$$

$$\sigma = \sigma(\varepsilon) = D\varepsilon, \text{ with } D = \frac{d\sigma}{d\varepsilon}(\varepsilon) \tag{2b}$$

in which D is the stiffness modulus defined by the stress level (see Fig.2(b)). Thus D can be either E the Young modulus, when the fiber is in the elastic range, $\sigma < \sigma_y$, where σ_y is the

yielding stress of steel; or E_t , the tangent modulus, when in the plastic range, $\sigma < \sigma_y$ (see Fig.2(c)). In case of elastic unloading, the stiffness modulus D assumes the value of the Young modulus E.

Applying the plastic-zone method, steel behavior can exhibit some other strain-hardening laws as shown in Fig.2(c). Additionally, to study the member behavior, the following hypotheses are considered:

i. the Bernoulli-Euler simplifications are adopted (all sections remain normal to FE's axis and cross-sections remain plane after loading application);

ii. the Poisson's effect is neglected;

iii. all members are braced out-of-plane (the generalized displacements and element forces are in plane only);

iv. the shear stress effect in yielding is disregarded;

v. all cross-sections are compact (WF profiles, which are not recommended for deep sections steel frames);

vi. all members are rigid connected and there is no finite node effect (panel distortion).

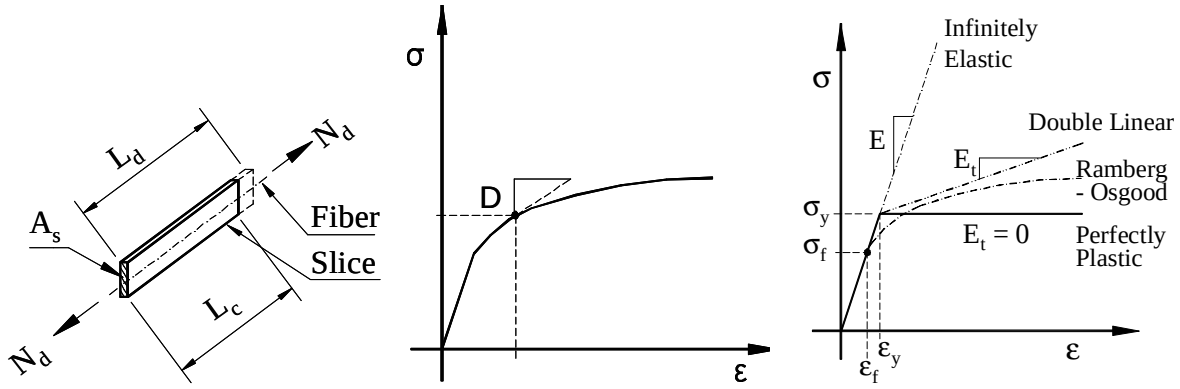

(a) Fiber stretching. (b) Stiffness modulus. (c) Some stress-strain laws.

Figure 2: Slice and fiber behavior.

Based on these hypotheses, elementary kinematics is applied accepting that any cross-section point's P behavior can be traced (stress and strain) by the cross-section's center *0*, which in turn (in elastic phase) is placed on the FE's axis. Then following Fig.3(a), the general P point displacements (u_d, v_d) can be related to the *0* centroid's displacements (u_{0d}, v_{0d}), by the following relations:

$$u_d(x, y_p) = u_{0d}(x) - y_p \sin \rho \tag{3a}$$

$$v_d(x, y_p) = v_{0d}(x) - y_p(1 - \cos \rho) \tag{3b}$$

in which x is the position of some section along the member (in the local system, in deformed configuration), and y_P is the distance between P point and *0* centroid.

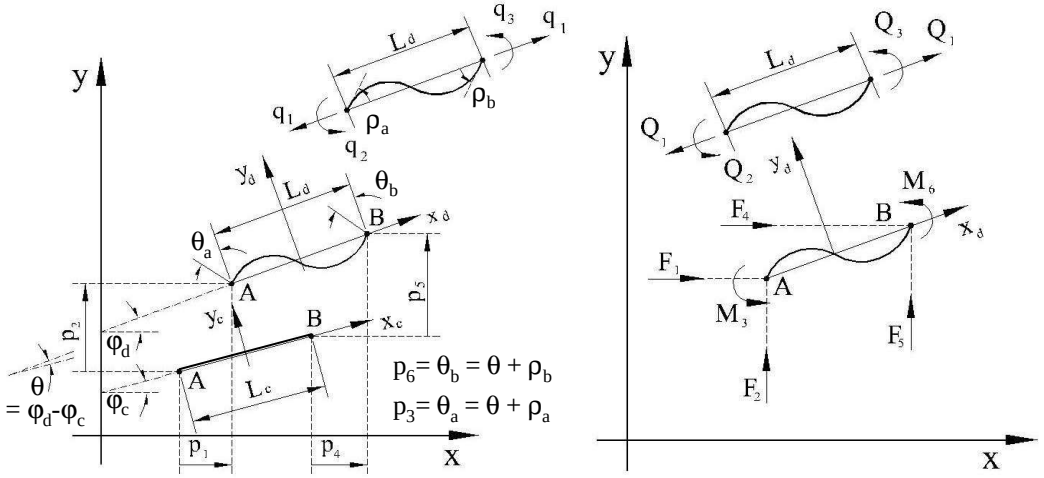

(a) Point P movement related to axis 0. (b) Specific rotation of the fiber.

Figure 3: Fiber and axis relationship.

Figure 3(b) shows a differential FE with length dx, closed by two end sections, where d is the section depth, R_{0d} is the section-axis curvature ratio and R_d is the curvature ratio of a fiber placed at generic point P. The elongation of the point P can be written as:

$$\varepsilon = \varepsilon_0 - y_p \rho' \tag{4}$$

in which ε_0 is the elongation of the axial fiber and ρ ' is the angle change of the chord joining the FE's ends in relation to the overall parallel x axis.

According to the geometry relations shown in figures, the secant approximation, combining Eqs. (1a) and (1b), and also assuming some simplifications ($\sin \rho \cong \tan \rho \cong \rho$, $\cos \rho \cong 1 - \rho^2/2$, $\sec \rho \cong 1 + \rho^2/2$), the basic relationship for the strain field in the numerical formulation is given by [2, 21, 27]:

$$\varepsilon = (1 + u'_{0d}) \left[1 + \frac{1}{2} \left(\frac{v'_{0d}}{1 + u'_{0d}} \right)^2 \right] - 1 - y_c \frac{v''_{0d}}{(1 + u'_{0d})} \tag{5}$$

where u_{0d} and v_{0d} are the FE axis' displacements and y_c is the centroid element coordinate which only coincides with y_r (reference coordinate, e.g. initial value) in the elastic range. When plasticity begins, the remaining elastic section's centroid does not necessarily coincide with the EF's axis, so the y_c value has to update for y_d at each iteration cycle.

Updated co-rotational Lagrangian formulation evaluates the strain field on the finite element movement. In the local co-rotational system, it defines three displacements as follows (see Fig.4(a)):

$$q_1 = L_d - L_c \tag{6a}$$

$$q_2 = \rho_a = \theta_a - \theta \tag{6b}$$

$$q_3 = \rho_b = \theta_b - \theta \tag{6c}$$

where the rotation $\theta = \varphi_d - \varphi_c$ is the FE's rigid body rotation, which is subtracted from θ_a and θ_b rotations to obtain q_2 and q_3 , while q_1 is the change of EF's chord length. An overall Cartesian system of the model describes these nodal motions permitting the conventional three degrees of freedom per node placed together in Fig.4(a), and is written as:

$$\text{Node } A : p_1 = u_a; p_2 = v_a; p_3 = \theta_a \tag{7a}$$

$$\text{Node } B : p_4 = u_b; p_5 = v_b; p_6 = \theta_b \tag{7b}$$

In the finite element context, u_{0d} and v_{0d} are provided by interpolating functions in the reference configuration. In traditional way, a linear function is chosen for u_{0d} and a third degree polynomial function for v_{0d} :

$$u_{0d}(x) \cong \Psi_1 q_1 \tag{8a}$$

$$v_{od}(x) \cong \left[1 + \frac{q_1}{L_r}\right] [\Psi_2 q_2 + \Psi_3 q_3] \tag{8b}$$

with

$$\Psi_1(x) = \frac{x}{L_r} + \frac{1}{2} \tag{9a}$$

$$\Psi_2(x) = \frac{8x^3 - 4L_r x^2 - 2L_r^2 x + L_r^3}{8L_r^2} \tag{9b}$$

$$\Psi_3(x) = \frac{8x^3 - 4L_r x^2 - 2L_r^2 x - L_r^3}{8L_r^2} \tag{9c}$$

2.2 Second-order inelastic stiffness matrix

Applying the Virtual Work Principle for the FE equilibrium on the reference volume V_r (initial), one can write:

$$\sum_{i=1 \text{ to } 6} P_i \delta p_i = \int_{V_r} \sigma \delta \varepsilon dV_r \tag{10}$$

As the change of $\delta\varepsilon$ can be expressed using the chain rule (assuming that ε is a function of q_α and also q_α is related to p_i), the following equilibrium relation is obtained:

$$P_i = \int_{V_r} \sigma \left(\frac{\partial \varepsilon}{\partial q_\alpha}\right)\left(\frac{\partial q_\alpha}{\partial p_i}\right) dV_r = Q_\alpha \left(\frac{\partial q_\alpha}{\partial p_i}\right) \tag{11}$$

being Q_α the co-rotational forces, which correspond to the six Cartesian forces shown in Fig.4(b).

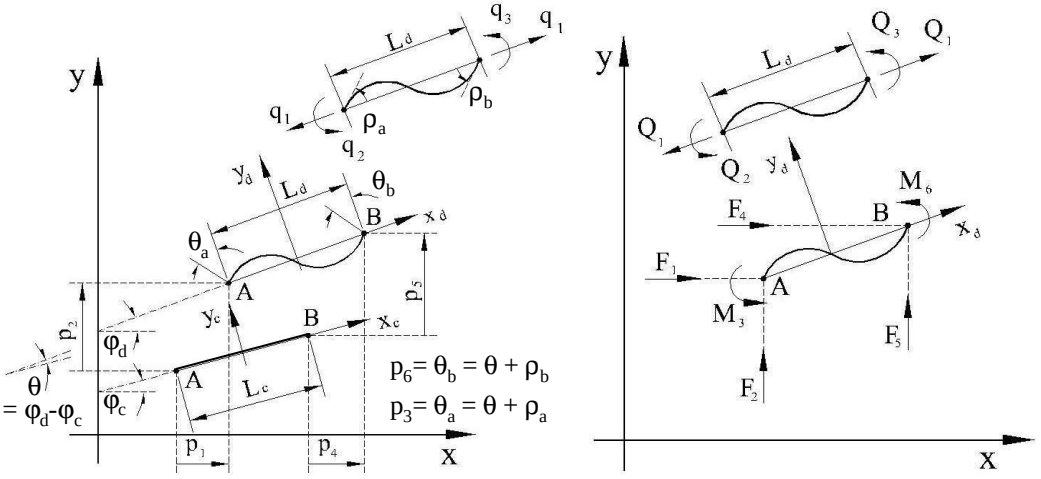

(a) General and co-rotational displacements. (b) Local and co-rotational forces.

Figure 4: Cartesian and co-rotational systems.

Thus, FE's stiffness matrix refereed to the overall system can be determined by the derivation of Eq. (11) in relation to a global displacement p_i . In this way:

$$K_{i,j} = \frac{\partial P_i}{\partial p_j} = \frac{\partial q_\alpha}{\partial p_i}\left(\frac{\partial Q_\alpha}{\partial q_\beta}\right)\frac{\partial q_\beta}{\partial p_j} + Q_\alpha \frac{\partial^2 q_\alpha}{\partial p_i \partial p_j} = \underbrace{q_{\alpha,i} D_{\alpha,\beta} q_{\beta,j}}_{\text{constitutive law}} + \underbrace{q_{\alpha,i} H_{\alpha,\beta} q_{\beta,j}}_{\text{curvature P}-\delta} + \underbrace{Q_\alpha q_{\alpha,ij}}_{\text{P}-\Delta\text{and M}-\Phi} \tag{12}$$

where:

$$D_{\alpha,\beta} = \int_{V_r} \left(\frac{\partial \varepsilon}{\partial q_\alpha}\right) D \left(\frac{\partial \varepsilon}{\partial q_\beta}\right) dV_r \tag{13a}$$

$$H_{\alpha,\beta} = \int_{V_r} \sigma \left(\frac{\partial^2 \varepsilon}{\partial q_\alpha \partial q_\beta} \right) dV_r \tag{13b}$$

$$q_{\alpha,ij} = \frac{\partial^2 q_\alpha(\varphi_d = 0)}{\partial p_i \, \partial p_j} \tag{13c}$$

The first term represents the constitutive law, while the others include second-order effects caused by FE's curvature (P-δ) and by both the P-Δ and M-Φ effects. Equation (12) can be rewritten in matrix notation as follows:

$$\mathbf{K} = \mathbf{K}_M + \mathbf{K}_H + \mathbf{K}_{G\alpha} \tag{14}$$

where $\mathbf{K}_M$ is the constitutive stiffness matrix and both $\mathbf{K}_H$ and $\mathbf{K}_{G\alpha}$ define the geometrical stiffness matrix. Numerical approximations provide the components of these matrices, and are given in the Appendix.

Finally, the structure stiffness matrix is built by summing the contribution of every element. As is usual in incremental analyses, some parts of the prescribed nodal loading are applied in steps. This process forms a set of linear equations, which is solved here by Gaussian reduction with backwards substitution [26]. With the displacements known, the stress and strain of every slice from each section (at nodes A or B) can be found and the internal forces evaluated. For the next iteration, the new loading uses the joint forces that were not equilibrated and the cycle stops only when equilibrium of the joint forces is attained (residual forces become negligible). In fact, this is the standard Newton-Raphson iterative strategy to solve nonlinear structural problems [26].

3 Axial force iterative integration (AFII)

According to Fig.5(a), if some fiber is in the elastic range, for a known strain ε_1 there is a stress $\sigma_1 < \sigma_y$, and $\varepsilon_1 = \sigma_1/E < \varepsilon_y$. In this case, the internal axial force $Q_1 = N_k$, with k node index equal to a or b, as shown in Fig 5(b)(I), where N_k is obtained by integrating all slices on side k of FE (see Appendix).

However, when a strain increment occurs like $\varepsilon_2 = \varepsilon_1 + d\varepsilon > \varepsilon_y$ at any load step of an incremental process, the new stress calculated by $\sigma_2 = \varepsilon_1 + Ed\varepsilon$ is greater than σ_y , therefore the fiber will be in the plastic range. There will be some plastic strain d p with an elastic strain $\varepsilon_y = \varepsilon_1 + d\varepsilon_e$ in such a way that $\varepsilon_2 = \varepsilon_y + d\varepsilon_p$. Figure 5(b)(II), for example, shows a FE where plasticity occurs at node A but the other side remains elastic (node B), and a strip plastic zone will appear along the FE. In this case, the internal axial force $N_a \neq N_b$. This creates a problem about Q_1 definition.

Based on the elastic-perfectly plastic material behavior shown in Fig.5(a), the plasticity of node A, for example, requires that σ_2 must be σ_y . Thus an unbalanced stress dσ will naturally appear, and now the vector Q_α (Q_1, Q_2 and Q_3) will show a difference in axial force,

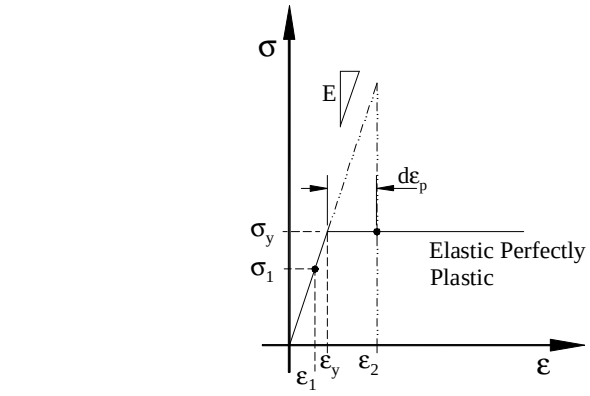

(a) Stress-strain diagram.

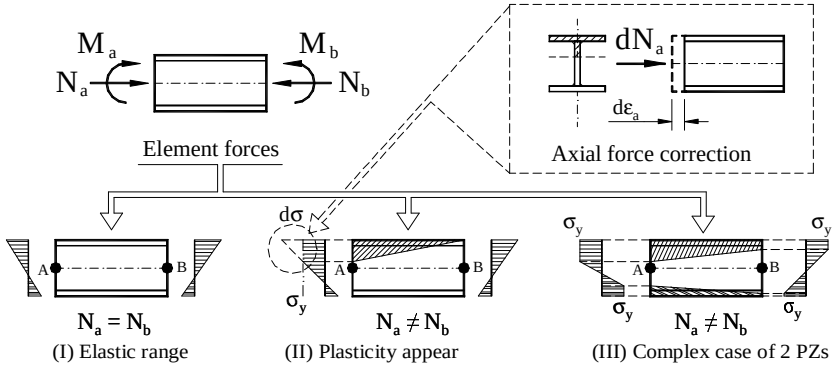

(b) Plastic-zone formation and dN correction.

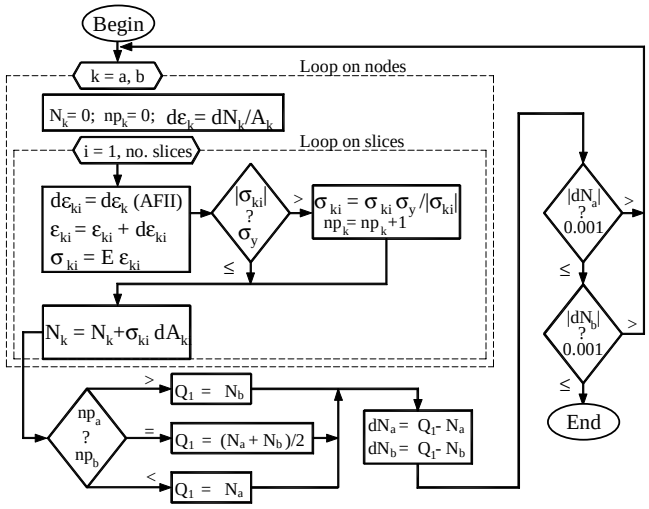

(c) Simplified flow-chart.

Figure 5: Axial force iterative integration.

$dN = N_a - N_b \neq 0$, which cannot be restored with the Newton-Raphson process only. For this reason, the present work proposes a new iterative process to adjust the stress and strain for all FEs with plasticity on any fiber. While the difference $|dN_k| >$ tolerance ($\cong 0.001$ kN) exists, a new axial strain on the node k index (a or b), where dN_k occurs, will be evaluated and is given by:

$$\delta\varepsilon_k = \frac{dN_k}{DA_{ck}} \tag{15}$$

in which A_{ck} is the section area in that iteration (current value), obtained at the node k index, that will be updated iteratively. Afterwards, the process finds a new stress, calculates new forces Q, and repeats the whole cycle until convergence. The goal of this procedure is to guarantee that each FE always verifies $Q_1 = N_a \cong N_b$, assuming the axial force must be constant (fixed between FE extremes). Figure 5(c) shows a simplified flow-chart of this iterative process, which can also solve more complicated cases like that of Fig.5(b)(III).

Moreover, the iterative integration procedure applied here brings the point with plasticity back to the yielding surface, correcting unavoidable distortions from the integrals of forces in plastic zone sections. This procedure is similar to what happens in the refined plastic-hinge approach, where a correction vector is used to keep the point on interaction surface (e.g. when axial force grows, it is necessary to reduce the plastic moment correspondingly [7, 23, 24]).

In the early stages of this formulation and computational program, the co-rotational axial force Q_1 was assumed to be a mean value of nodal integrated forces N_a and N_b . Using this mean value results in unwanted differences afterwards, and this justifies the present proposal.

4 Examples of validation

Three validation examples are presented. The first investigates a beam-column with member's out-of-straightness; the second shows the results obtained using the two strategies to evaluate the axial force component Q_1 (with and without the axial force iterative-integration proposed); and the third, it is the famous Vogel's portal frame, that is usually adopted for calibrating advanced second-order inelastic analysis.

4.1 Galambos-Ketter's beam-column

Chen *et al.* [9] pointed out the structural problem illustrated in Fig.6 as a benchmark problem for second-order inelastic analysis. The goal is to verify the interaction between the axial force and end moments at collapse, for different values of slenderness ratio L/r_z , in which L is the column length and r_z is the radius of gyration of the cross sectional area surrounding the centroidal axis. Figure 6 also presents the corresponding data, where only the case with no residual stress was considered. A companion paper studies the case with residual stress.

Figure 7 demonstrates the good agreement between the answers from the present work and

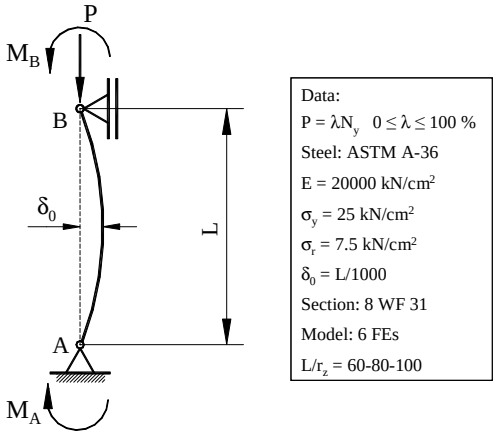

Figure 6: Galambos and Ketter's beam-column.

those produced by the BCIN program [9,11]. The latter also performed a plastic-zone approach but with the finite difference method and using a mesh of 20 sections, having both flange and web divided into 40 strips and an initial out-of-straightness $\delta_0 = 0.5$ mm at the middle length. This work considered a mesh with only 6 FEs to model the beam-column, and the half-flanges and the web were divided into 20 and 36 slices, respectively.

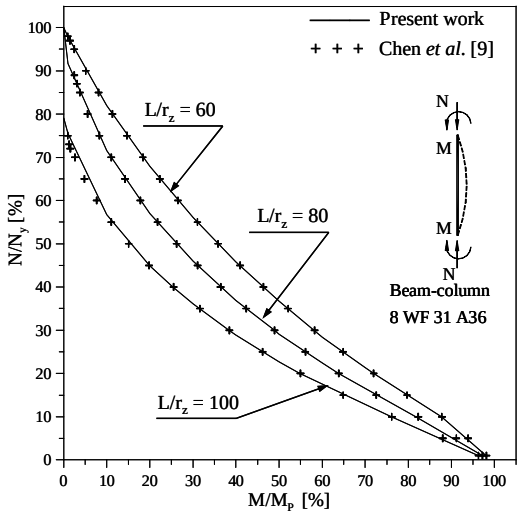

Figure 7: Galambos and Ketter beam-column's interaction diagram.

4.2 Galambos' portal frame

Figure 8 shows the steel portal frame studied by Galambos [14] and also adopted to validate the slices technique formulation [21]. The frame's equilibrium paths are presented in Fig.9, showing the results obtained by using two different strategies to evaluate the element axial force, i.e., with and without the axial force iterative integration proposed. In the last case, a mean value of the element end axial forces was assumed [21].

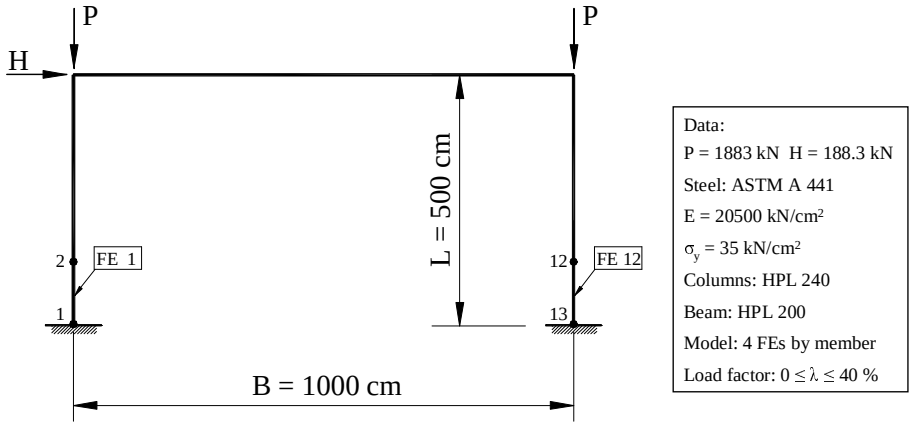

Figure 8: Galambos' portal frame equilibrium path.

The equilibrium paths computed by the *axial force iterative integration* (AFII) and *axial force mean* (AFM) are very close to the answers by Galambos as displayed in Fig.9. The collapse loads, presented in Tab. 1 with the drift u_{An} prior collapse, show close agreement as well. Nevertheless, it is worth mentioning that when the structural collapse is caused by inelastic buckling instead of incomplete plastic mechanism formation, the numerically determined collapse load by the AFM strategy tends to be a little bigger and the equilibrium path increases a little, too. Figure 9 illustrates this behavior.

Table 2 shows the internal forces near collapse load on elements 1 and 12 obtained by AFII and AFM. While the first has the same value for axial forces ($N_a \cong N_b$) the latter has different ones ($N_a < N_b$). In this example, plasticity only happens at node A, while node B remains elastic at that selected FE. This drawback can only be detected when the integrated axial forces are printed. Moreover, Tab. 2 shows that not only the N_a and N_b values are different when using AFM, but also the bending moments in the plastic-zone nodes (1 and 12) are bigger than expected. In contrast, on the other end (2 and 11 nodes), forces continue to grow reaching plasticity. Briefly: the axial force begins to reduce in node A and to grow at node B as the Newton-Raphson iterations develop and the moment is not reduced in those plastic zones as would be expected!

Finally, the difference dN tends to be larger as the plasticity and load step increases, which justifies the present work contribution. Using the AFII procedure, the iterations stop when

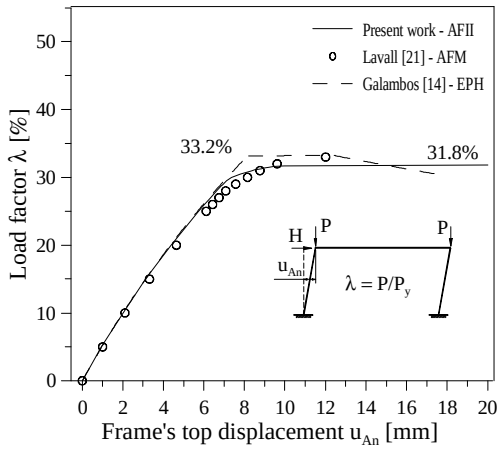

Figure 9: Galambos' portal frame.

Table 1: Galambos' frame: collapse load factor and drift.

Galambos [14] EPH[4]		Lavall [21] PZ		Present Work PZ	
λ [%]	u_{An} [cm]	λ [%]	u_{An} [cm]	λ [%]	u_{An} [cm]
31	7.464	31.0	8.769	31	8.378
32	7.780	32.0	9.615	31.7	9.965
33.2	8.167	33.0	12.006	31.8[3]	33.633
30.47[1]	17.50	34.0[2]	-	-	-

Notes: 1. Galambos does not define collapse-load; 2. No further information;
3. Matrix shows singularity, last iteration's drift u_{An} is given;
4. EPH: second-order elastic-plastic hinge.

Table 2: Galambos' frame: forces near collapse.

$\lambda^{(1)}$ [%]	FE	Node[2]		AFM: Axial Force Mean[6]						**AFII: Axial Force Iterative Integration**		
		A	B	N_a [kN]	N_b [kN]	M_a [kNcm]	M_b [kNcm]	dN[3] [kN]	$Q_1^{(4)}$ [kN]	$N_a = N_b$ [kN]	M_a [kNcm]	M_b [kNcm]
30	1	1	2	543.426	553.649	10244.0	6156.9	-10.223	548.538	548.505	10254.7	6161.0
	12	12	13	573.641	587.978	6090.5	10114.3	14.337	580.810	580.840	6075.6	10100.0
31	1	1	2	555.816	575.879	10681.3	6340.0	-20.063	565.848	565.657	10684.3	6319.3
	12	12	13	588.273	613.813	6231.0	10490.1	**25.540**	**601.043**	601.214	6194.0	10471.2

Notes: 1. The collapse occurs at $\lambda = 31.8$;
2. Plasticity appear at nodes 1 and 13 only, while nodes 2 and 12 remain elastic;
3. dN=$N_a - N_b$; 4. $Q_1 = (N_a + N_b)/2$
5. Max. difference (corresponds to bold values) is dN/Q_1= 5.37%;
6. AFM results obtained by present work computational program.

the absolute value of dN $\geq$ 0.001 kN or when a given number of cycles (200 adopted here) are performed without convergence.

4.3 Vogel's portal frame

Figure 10 [31] shows this portal frame and all required data. The European rolled shapes were used considering ECCS [12], with a residual stress of $\sigma_r = 0.5\ \sigma_y$. Furthermore, the structural model, as required by advanced analysis, includes the out-of-plumbness Δ_0 = L/400 and the out-of-straightness σ_0 = L/1000 for both columns. Since the frame collapse is determined by the column's inelastic buckling, this example is a good benchmark test for any inelastic formulation [11].

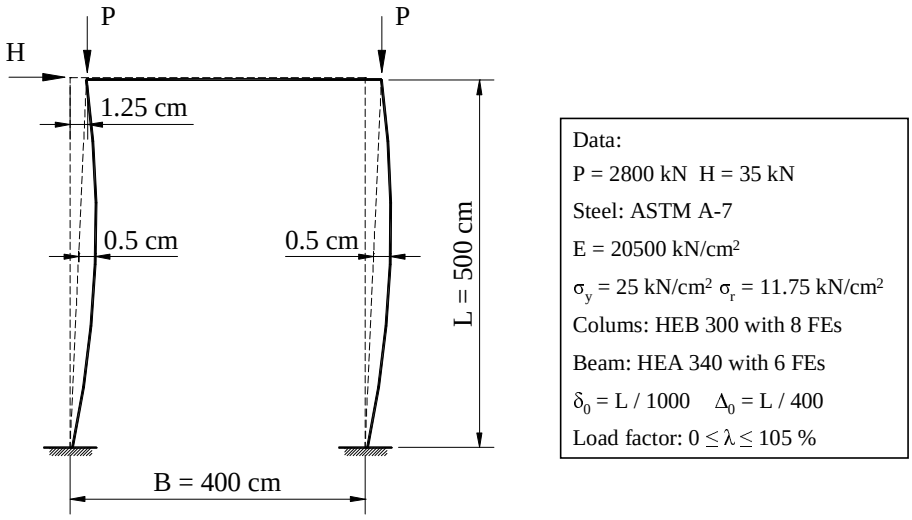

Figure 10: Vogel's portal frame.

Ziemian *et al.* [33] and Clarke [11], both applying PZ formulation, adopted 120 elements (50 FEs by column). Based on plastic-hinge methodology, Teh and Clarke [29] and Machado [24] used four FEs for the whole structure. There is not much details about Liew's FE model, who used the refined plastic-hinge and notional load approaches [9]. Avery and Mahedran [4], and Kim and Lee [19], using the Abacus commercial software, modeled the frame with 8952 3D-shell elements. Chan and Zhou [8] adopted the coarsest mesh (one FE by member) and the refined plastic-hinge method with a high-order polynomial function called PEP.

Table 3 displays the collapse load factor λ_{col} and the column top horizontal displacement u_{An} . This table shows that displacements ranging from 14.2 to 17.3 mm are a good response and the present work's value falls within this range.

Figure 11 illustrates the Vogel's frame nonlinear equilibrium path obtained by some researchers. Notice that present work's results agree well with the Vogel's path, yet both are above Machado's refined plastic-hinge analysis. Table 4 demonstrates the element forces at the

Table 3: Vogel's frame: collapse load factor and drift

Collapse point	Vogel [31]		Ziemian [33]		Clarke [11]	Chen *et al.* [9]	
	PZ	EPH	PZ	RPH	PZ	NL-PH	RPH
λ_{col} [%]	102.2	101.7	99.9	105.0	102.3	99.9	96.0
u_{An} [mm]	17.3	11.5	14.2	12.0	17.1	12.9	14.8
Collapse point	Teh and Clarke [29]	Avery and Ma-hendran [4]	Kim and Lee [19]	Chan and Zhou [8]	Machado [24]		**Present Work**
	PZ	PZ	PZ	PEP	RPH	AS-PH	**PZ**
λ_{col} [%]	100.5	101.0	103.0	103.3	94.0	98.0	100.7
u_{An} [mm]	20.0	16.2	19.2	16.0	17.01	32.56	17.00

Notes on methods: PZ - plastic zone; EPH - second-order elastic-plastic hinge;
RPH - refined plastic hinge; NL-PH - notional load plastic hinge;
PEP - polynomial enhanced plastic hinge; AS-PH - assembly section plastic hinge [6]

collapse load, in which N is the axial force, Q the horizontal shear, and M the bending moment. The subscript letters mean: (A) left column, (B) beam and (C) right column, (1) base node and (n) columns top node. The present work's values are again near Vogel's and Ziemian's, both with PZ formulation, and show a slight difference in relation to the other researchers' answers.

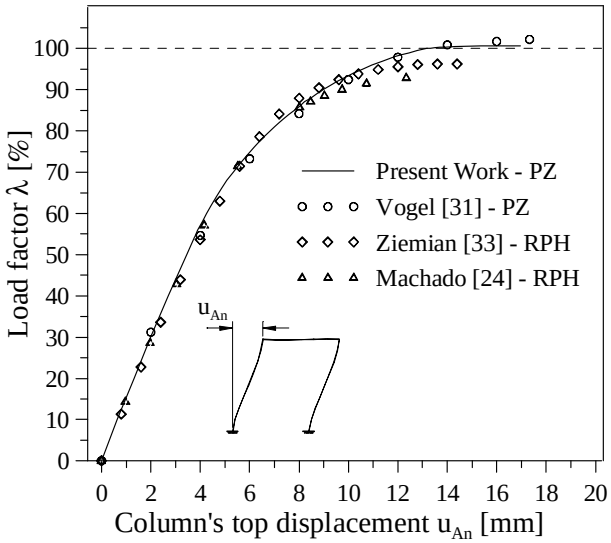

Figure 11: Vogel portal frame's equilibrium path.

The explanation for this variety of answers is in Fig.12, which shows the yielded slice diagram of the structure near the collapse load. As displayed, there are two plastic zones in each column,

Table 4: Vogel's frame: forces near collapse.

Forces[(1)]		Vogel [31] PZ	Ziemian [33] PZ	Clarke [11] PZ	Chen *et al.* [9] RPH	Chen *et al.* [9] NL-PH	Machado [24] AS-PH	Present Work PZ
N_A	[kN]	2770.2	2765.0	2821.0	2649.0	2752.0	2711.0	2780.7
N_C		2829.9	2843.0	2905.0	2721.0	2846.0	2791.0	2858.5
N_B		13.4	-	-	-	-	-	15.8
Q_1		30.8	-	-	-	-	-	40.5
Q_n		28.4	-	-	-	-	-	21.7
M_{A1}	[kNcm]	9071.0	8703.0	9385.0	8586.0	10600.0	9248.0	9854.4
M_{An}		7464.0	7955.0	8721.0	7357.0	9580.0	8174.0	8058.1
M_{C1}		9055.0	8242.0	8277.0	8389.0	9270.0	8784.0	8832.1
M_{Cn}		7462.0	7573.0	8084.0	7069.0	9207.0	7804.0	7492.7
λ_{col}		1.022	0.999	1.023	0.960	1.040	0.980	1.007
FE/col.		-	50	50	1	1	1	8

Notes: 1. Indexes: A and C for left and right column, B for beam, 1 and n for first and last nodes in the member;
2. some values are not given in the existing literature.

created by compression along the member, and no yielding occurs in the beam. These two columns' plastic-zones seem to be equal, and the collapse happens by inelastic instability.

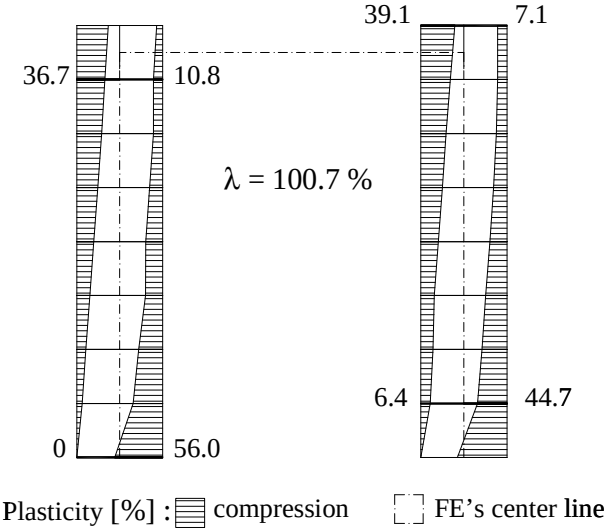

Figure 12: Vogel portal frame's plastic zones.

5 Final remarks

A numerical procedure involving a second-order inelastic analysis of steel structures using the plastic-zone method and producing a new axial force iterative integration procedure is presented in this paper. The slice technique is the base for the plastic-zone formulation adopted. All three studied benchmark problems presented good agreement with those found in literature. This seems to validate the proposed formulation.

It is worth noting that the proposed numerical methodology was able to trace what occurs inside the steel section and along the member, which means the identification of the start and spread of plasticity. Therefore, this formulation can supply a more comprehensive investigation on the strength and stability of the steel structures.

Based on the nonlinear analysis carried out here and other already-solved steel frame problems, when comparing the proposed numerical methodology with other formulations or methods, the following comments can be made:

i. the quality and precision of the obtained responses are equivalent to those obtained from Abaqus or Ansys 3D plastic zone solutions, even using a more simplified model;

ii. once considered as one more precise numerical formulation, our responses can be used to validate refined plastic-hinge computational implementations, which naturally have difficulties with plasticity spread simulation but do not require too much computer work; and

iii. when compared with others plastic zone approaches, the proposed axial force iterative integration maintains the quality of the internal force recovery, more precisely determining the plasticity spread and for this reason a better answer is obtained.

These comments justify and even make attractive the development of this line of research.

In spite of this, it should be mentioned that there is a long road ahead in making this process available for offices. For example, some cases of load increment strategies can lead the solution toward stationary points, among other critical points. In seeking completeness, this method also deserves improvement to fulfill the design needs of non-linear connection behavior, as well as 3D analysis.

Besides, the plastic-zone analysis often requires more computer memory, speed and a great amount of time. The development of more powerful languages and computer resources are needed for this kind of approach to become useful and attractive for office projects. Foley [13], for example, applied parallel processing and vectorization to improve the computational process. Nevertheless, the authors hope that forthcoming research will usher in new ways to make this more affordable and that the simple shape used here can be expanded to a powerful one in the near future.

6 Acknowledgments

The authors are grateful for the financial support from the Brazilian National Council for Scientific and Technological Development (CNPq/MCT), CAPES and the Minas Gerais Research Foundation (FAPEMIG). They also acknowledge the support from the Brazilian Steel Company USIMINAS for this research. Special thanks go to Professor Michael D. Engelhard from University of Texas at Austin for his valuable suggestions; and John White and Harriet Reis for their editorial reviews.

References

[1] AS 4100. *Steel structures*. Standards Association of Australia, Sidney, Australia, 1990.

[2] A.R. Alvarenga. Main aspects in plastic-zone advanced analysis of steel portal frames. M.Sc. thesis, Civil Engineering Program, EM/UFOP, Ouro Preto, MG, Brazil, 2005. (in Portuguese).

[3] A.R. Alvarenga and R.A.M. Silveira, editors. *Considerations on Advanced Analysis of Steel Portal Frames, Proceedings of ECCM III European Conference on Computational Mechanics Solids, Structures and Coupled Problems in Engineering*, Lisbon, Portugal, 2006. pp 2119.

[4] P. Avery and M. Mahendran. Distributed plasticity analysis of steel frame structures comprising non-compact sections. *Engineering Structures*, 22:901–919, 2000.

[5] R. Bjorhovde. Effect of end-restraint on column strength – practical applications. *AISC Engineering Journal*, 1:1–13, 1984.

[6] S.L. Chan and P.P.T. Chui. A generalized design-based elastoplastic analysis of steel frames by section assemblage concept. *Engineering Structures*, 19(8):628–636, 1997.

[7] S.L. Chan and P.P.T. Chui. *Nonlinear static and cyclic analysis of steel frames with semi-rigid connections*. Elsevier, Oxford, 2000.

[8] S.L. Chan and Z.H. Zhou. Elastoplastic and large deflection analysis of steel frames by one element per member, ii: Three hinges along member. *Journal of Structural Engineering ASCE*, 130(4):545–553, 2004.

[9] W.F. Chen, Y. Goto, and J.Y.R. Liew. *Stability design of semi-rigid frames*. John Willey and Sons, New York, 1996.

[10] W.F. Chen and E.M. Lui. *Structural stability – theory and implementation*. Elsevier, New York, 1987.

[11] M.J. Clarke. Plastic zone analysis of frames. In W.F. Chen and S. Toma, editors, *Advanced analysis of steel frames: theory, software and applications*. CRC Press, Boca Raton, 1994.

[12] ECCS. Ultimate limit state calculations of sway frame with rigid joints. Technical working group 8.2, publication 33, European Convention for Constructional Steelwork, Brussels, 1984.

[13] C.M. Foley. Advanced analysis of steel frames using parallel processing and vectorization. *Computer-Aided Civil and Infrastructure Eng.*, 16:305–325, 2001.

[14] T.V. Galambos. *Structural Members and Frames*. Dept. Civil Engineering, Un. Minnesota Mineapolis, 1982.

[15] T.V. Galambos and R.L. Ketter. Columns under combined bending and thrust. *Transations ASCE*, 126(1):1–25, 1961. New York, 1959.

[16] J.F. Hajjar. *Effective length and notional load approaches for assessing frame stability: Implications for American steel design, Task Committee on Effective Length of the Technical Committee on Load and Resistance Factor Design of the Technical Division of the Structural Engineering*. Institute of the American Society of Civil Engineers, Reston, Va., 1997.

[17] J.F. Hajjar and D.W. White. Stability of steel frames: the cases for simple elastic and rigorous inelastic analysis - design procedure. *Engineering Structures*, 22:155–167, 2000.

[18] S.E. Kim, M.K. Kim, and W.F. Chen. Improved refined plastic hinge analysis accounting for strain reversal. *Engineering Structures*, 22:15–25, 2000.

[19] S.E. Kim and D.H. Lee. Second-order distributed plasticity analysis of space steel frames. *Engineering Structures*, 24:735–744, 2002.

[20] A. Landesmann. Analysis and implementation of plastic model for steel framed structures. M.Sc. thesis, Civil Engineering Program/COPPE/UFRJ, Rio de Janeiro, RJ, Brazil, 1999. (in Portuguese).

[21] A.C.C. Lavall. *A consistent theory formulation for non-linear analysis by finite element method considering initial imperfections and residual stress in cross section*. D.Sc. Dissertation, EESC/USP, São Carlos, SP, Brazil, 1996. (in Portuguese).

[22] W.J. LeMesurier, editor. *Simplified K-factors for stiffness controlled designs*, 1797-1812, New York, 1995.

[23] J.Y.R. Liew, D.W. White, and W.F. Chen. Second-order refined plastic-hinge analysis for frame design. parts i and ii. *Journal of Structural Engineering, ASCE*, 119(11):3196–3237, 1993.

[24] F.C.S. Machado. Second-order inelastic analysis of steel structured systems. M.Sc. thesis, Civil Engineering Program EM/UFOP, Ouro Preto, MG, Brazil, 2005. (in Portuguese).

[25] American Institute of Steel Construction. *Specification for structural steel buildings*. AISC, Chicago, 2005.

[26] D.R.J. Owen and E. Hinton. *Finite elements in plasticity: theory and practice*. Pineridge Press Ltd, Swansea, UK, 1980.

[27] R.J. Pimenta. Proposition of buckling curve for welded wf built from fire cut plates. M.Sc. thesis, Federal University of Minas Gerais, Belo Horizonte, MG, Brazil, 1996. (in Portuguese).

[28] F.C. Siat-Moy. K-factor paradox. *Journal of Structural Engineering ASCE*, 112(8):1747–1760, 1986.

[29] L.H. Teh and M.J. Clarke. Plastic-zone analysis of 3d steel frames using beam elements. *Journal of Structural Engineering ASCE*, 125(11):1328–1337, 1999.

[30] S. Vinnakota and C.M. Foley. Inelastic behavior of multistory partially restrained steel frames. parts i and ii. *Journal of Structural Engineering ASCE*, 125(8):854–868, 1999.

[31] U. Vogel. Calibrating frames. *Stahlbau*, 10:295–301, 1985.

[32] R.D. Ziemian and W. McGuire. Modified tangent modulus approach, a contribution to plastic hinge analysis. *Journal of Structural Engineering ASCE*, 128(10):1301–1307, 2001.

[33] R.D. Ziemian, W. McGuire, and G.G. Deierlein. Inelastic limit state design, part i: Planar frames studies; part ii: Three-dimensional frame study. *Journal of Structural Engineering ASCE*, 118(9):2352–2568, 1992.

Appendix: The finite element matrices and numerical integration

$$K_M = \begin{bmatrix} \frac{D_{1m}}{L_r} & 0 & \frac{D_{2m}}{L_r} & -\frac{D_{1m}}{L_r} & 0 & \frac{D_{2m}}{L_r} \\ & \frac{12D_{3m}}{L_r L_d^2} & \frac{6D_{3m}}{(L_r L_d)} & 0 & -\frac{12D_{3m}}{(L_r L_d^2)} & \frac{6D_{3m}}{(L_r L_d)} \\ & & \frac{4D_{3m}}{L_r} & \frac{D_{2m}}{L_r} & -\frac{6D_{3m}}{(L_r L_d)} & \frac{2D_{3m}}{L_r} \\ & & & \frac{D_{1m}}{L_r} & 0 & -\frac{D_{2m}}{L_r} \\ & & & & \frac{12D_{3m}}{(L_r L_d^2)} & -\frac{6D_{3m}}{(L_r L_d)} \\ \text{sim.} & & & & & \frac{4D_{3m}}{L_r} \end{bmatrix} \tag{16}$$

$$K_H = \begin{bmatrix} 0 & 0 & 0 & 0 & 0 & 0 \\ & \frac{Q_1}{5L_d} & \frac{Q_1}{10} & 0 & -\frac{Q_1}{5L_d} & \frac{Q_1}{10} \\ & & \frac{2Q_1 L_d}{15} & 0 & -\frac{2Q_1}{15} & -\frac{Q_1 L_d}{30} \\ & & & 0 & 0 & 0 \\ & & & & \frac{Q_1}{5L_d} & -\frac{Q_1}{10} \\ \text{sim.} & & & & & \frac{2Q_1 L_d}{15} \end{bmatrix} \tag{17}$$

$$K_{G\alpha} = \begin{bmatrix} 0 & \frac{Q_2+Q_3}{L_d^2} & 0 & 0 & -\frac{Q_2+Q_3}{L_d^2} & 0 \\ & \frac{Q_1}{L_d} & 0 & -\frac{Q_2+Q_3}{L_d^2} & -\frac{Q_1}{L_d} & 0 \\ & & 0 & 0 & 0 & 0 \\ & & & 0 & \frac{Q_2+Q_3}{L_d^2} & 0 \\ & & & & \frac{Q_1}{L_d} & 0 \\ \text{sim.} & & & & & 0 \end{bmatrix} \tag{18}$$

The FE matrices have terms related to deformed length (L_d), which changes at each iterative step, and also to initial or reference length (L_r), which is fixed from the beginning of the analysis. Besides the co-rotational forces Q_1 , Q_2 and Q_3 , there are the terms D_{1m} , D_{2m} and D_{3m} that represent the elastic-plastic geometrical properties of the section to be evaluated at each step of the incremental-iterative process. These geometrical properties are obtained by average values using:

$$D_{jm} = 0.5(D_{ja} + D_{jb}), \text{ with } j = 1, 2, 3 \tag{19}$$

where D_{jk} is evaluated at the k node index (a or b) as follows:

$$D_{jk} = \int_{A_r} D(y_c)^{(j-1)} dA_r = \sum_{i=1}^{\text{no. slices}} \left[D_i (y_{ci})^{(j-1)} dA_{ri} \right] \tag{20}$$

in which D_{1k} , D_{2k} and D_{3k} are evaluated numerically by DdA, $Dy_c dA$ and $Dy_c{}^2 dA$ integration, respectively.

The co-rotational axial force on FE is defined by the new process proposed: Q_1 = AFII (N_a, N_b), where AFII is the Axial Force Iterative Integration applied to the axial forces N_a and N_b obtained from integration on k node index (a or b), respectively, using the expression:

$$N_k = \int_{A_r} \sigma dA_r = \sum_{i=1}^{\text{no. slices}} [\sigma_i \, dA_{ri}] \tag{21}$$

in such way that these integrals have the same value as Q_1 .

The co-rotational moments Q_2 = -M_a and Q_3 = M_b , are also given by:

$$M_k = \int_{A_r} \sigma y_c dA_r = \sum_{i=1}^{\text{no. slices}} [\sigma_i y_{ci} \, dA_{ri}] \tag{22}$$